## Technical Note

# T2-Weighted Prostate MRI at 7 Tesla Using a Simplified External Transmit-Receive Coil Array: Correlation With Radical Prostatectomy Findings in Two Prostate Cancer Patients

Andrew B. Rosenkrantz, MD,[1]* Bei Zhang, PhD,[1] Noam Ben-Eliezer, PhD,[1]
Julien Le Nobin, MD,[2] Jonathan Melamed, MD,[3] Fang-Ming Deng, MD, PhD,[3]
Samir S. Taneja, MD,[2] and Graham C. Wiggins, DPhil[1]

**Purpose:** To report design of a simplified external transmit-receive coil array for 7 Tesla (T) prostate MRI, including demonstration of the array for tumor localization using T2-weighted imaging (T2WI) at 7T before prostatectomy.

**Materials and Methods:** Following simulations of transmitter designs not requiring parallel transmission or radiofrequency-shimming, a coil array was constructed using loop elements, with anterior and posterior rows comprising one transmit-receive element and three receive-only elements. This coil structure was optimized using a whole-body phantom. In vivo sequence optimization was performed to optimize achieved flip angle (FA) and signal to noise ratio (SNR) in prostate. The system was evaluated in a healthy volunteer at 3T and 7T. The 7T T2WI was performed in two prostate cancer patients before prostatectomy, and localization of dominant tumors was subjectively compared with histopathological findings. Image quality was compared between 3T and 7T in these patients.

**Results:** Simulations of the $B_1^+$ field in prostate using two-loop design showed good magnitude ($B_1^+$ of 0.245 A/m/w$^{1/2}$) and uniformity (nonuniformity [SD/mean] of 10.4%). In the volunteer, 90° FA was achieved in prostate using 225 v 1 ms hard-pulse (indicating good efficiency), FA maps confirmed good uniformity (14.1% nonuniformity), and SNR maps showed SNR gain of 2.1 at 7T versus 3T. In patients, 7T T2WI showed excellent visual corre-

spondence with prostatectomy findings. 7T images demonstrated higher estimated SNR (eSNR) in benign peripheral zone (PZ) and tumor compared with 3T, but lower eSNR in fat and slight decreases in tumor-to-PZ contrast and PZ-homogeneity.

**Conclusion:** We have demonstrated feasibility of a simplified external coil array for high-resolution T2-weighted prostate MRI at 7T.

**Key Words:** prostate cancer; MRI; T2-weighted imaging; 7T; coil
**J. Magn. Reson. Imaging 2013;00:000–000.**
© 2013 Wiley Periodicals, Inc.

MRI OF THE prostate is being increasingly used for a variety of clinical purposes, including tumor detection and localization, treatment planning, and assessment of aggressiveness (1). These assessments have traditionally relied upon a combination of high-resolution turbo spin-echo T2-weighted imaging (T2WI) and additional functional sequences, including diffusion-weighted imaging, dynamic contrast-enhanced imaging, and MR spectroscopy. The emergence of 3 Tesla (T) MR systems over the past decade has facilitated improvements in the image quality of these sequences (2), such that 3T systems are now routinely used for prostate MRI at many centers.

More recently, some centers have acquired 7T systems that offer the possibility of imaging prostate tumors using contrast mechanisms that have not been reliably performed at 1.5T and 3T, such as arterial-spin labeling (3) and multinuclear imaging (4). Before integrating such techniques into a potential clinical MR examination at 7T, it is first necessary to be able to perform standard MR sequences at diagnostic quality at this field strength; this task is not a straightforward matter. Extreme inhomogeneity of the radiofrequency (RF) transmit field in body applications at 7T creates a large challenge in imaging a structure located deep in the torso, such as the

**Figure 1.** An eight-element prostate coil (T/R: transmit and receive; R: receive only). System comprises anterior and posterior rows, each containing four overlapping coil elements: one T/R element and three R elements.



**Figure 2.** Combined $B_1^+$ field for two offset loop system, showing region of sufficiently uniform excitation in the prostate achieved using this coil arrangement.

prostate. This inhomogeneity, combined with the significantly increased power deposition, has generally precluded use of whole-body transmit coils at 7T (5), as is the norm at 1.5T and 3T. Rather, local transmit coils, also serving as receiver coil elements, must be used for 7T imaging of the torso. Yet, highly complex $B_1^+$ fields and the greater power deposition at 7T similarly have lead to great difficulty in the development of safe high-performance local transmit-receiver coil arrays for imaging of the prostate, as well as of the torso in general, at 7T. Indeed, to our knowledge, T2WI of prostate tumors in humans at 7T has not been previously published in the peer-reviewed literature.

One group has demonstrated the application of 8- and 16-channel transmit-receive coil arrays for prostate MRI at 7T in healthy volunteers (5,6). However, this system relied on parallel transmission and RF shimming, a cumbersome process that brings even greater complexity to the hardware requirements and data acquisition of an already highly complex challenge. Given that the prostate occupies only a small area of interest within the pelvis, we propose that sufficiently homogeneous excitation in the prostate may be achieved through the use of only two transmitter elements (one anterior and one posterior, with fixed power split and phase relationship), which if positioned appropriately should interfere constructively in the prostate, thereby avoiding the need for parallel transmission and RF shimming. This approach is hoped to provide a simple solution for obtaining high-quality T2WI of the prostate at 7T. Thus, our aim in this study was to design a simplified external transmit-receive coil array for 7T prostate MRI, and to demonstrate this array for tumor localization using T2-weighted imaging (T2WI) at 7T before radical prostatectomy.

## MATERIALS AND METHODS

### Simulations and Phantom Studies

The strong interaction between human tissue and the electromagnetic (EM) field requires full wave EM simulation to predict the coil behavior. A system with two surface coil loops was simulated with the finite-difference time-domain (FDTD) method (Microwave
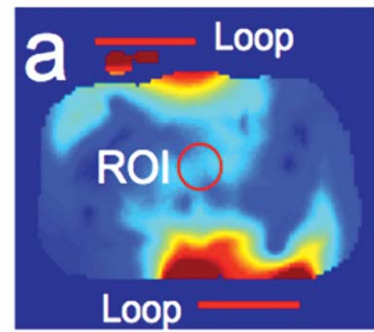
Studio, CST, Germany). The simulated loop diameter was 16cm, corresponding to the approximate depth of the region-of-interest (ROI) in the HUGO body model. One loop is placed anterior and the other is placed posterior, with both loops shifted 5.5 cm away from the center in opposite directions to compensate for $B_1^+$ twisting (7,8) to create maximum $B_1^+$ in the ROI. Based on the simulation results, a coil array for in vivo imaging was subsequently constructed using loop elements, with a row of four overlapped anterior elements and another row of four overlapped posterior elements (Fig. 1). The loop diameter was reduced to 12 cm based on phantom experiments. In each row of four elements, one coil was used to both transmit and receive, while the remaining three coils were receive-only. A quarter lambda lattice balun was constructed at the output of each loop to balance current flowing in the coil. Each receive-only element was connected to a preamplifier (Siemens Healthcare, Erlangen, Germany) and preamp decoupling was implemented with a phase shifter to transform the input impedance of the preamp appropriately. Bridging the lattice balun with a diode provided active detuning, and additional detuning was provided by a passive detuning circuit located on the opposite side of the loop. For the two transmit-receive elements, equal power was provided to each coil through a Wilkinson power divider, with cable lengths chosen to provide $180°$ phase difference between the two coils. A T/R switch was placed in each transmit path, routing the coils either to the RF transmitter or to two preamps. To allow conformation of the anterior array to different subjects, it was constructed of a single piece of etched Pyralux flexible circuit board material (Dupont, Wilmington DE).

Experimental measurements of the performance of this coil array were performed using a body-sized tissue-equivalent phantom, that allowed further optimization of the 2 loop transmit structure. In addition, temperature tests were conducted with meat to determine safe specific-absorption ratio (SAR) limits.

### Volunteer Evaluation

Given the challenge in creating sufficient excitation in the prostate in vivo with the 8 kW total RF

Table 1
Image Parameters for Axial T2-Weighted Imaging of the Prostate at 3T and 7T

| Field strength | TR(ms) | TE(ms) | FA | ST(mm) | FOV(mm) | Matrix | BW(Hz/vox) | Averages | Parallel imaging |
|---|---|---|---|---|---|---|---|---|---|
| 3T | 4,960 | 105 | 150 | 3 | $180 \times 180$ | $256 \times 256$ | 201 | 3 | 2 |
| 7T | 11,670 | 80 | 160 | 3 | $192 \times 192$ | $256 \times 256$ | 254 | 1 | None |

power available from scanner RF amplifiers, further sequence optimization was performed. These sequence modifications were aimed toward increasing the flip angle in the prostate while staying within the available RF pulse voltage limit. Sequence modifications comprised: (i) extending the 180 degree RF pulse duration to reduce pulse amplitude needed for a given flip angle; this modification generated significantly higher SNR within the prostate; (ii) extending the 90-degree RF pulse duration; and (iii) using RF pulses with lower time-bandwidth-product; this change trades the slice profile for lower pulse power, enabling further power for a given SAR.

A 29-year-old healthy male volunteer was evaluated using this coil-array, after providing written informed consent as part of a prospective Institutional Review Board (IRB) -approved HIPAA-compliant study. Flip angle maps were obtained with a turboFLASH sequence using preparation pulses (repetition time/echo time/bandwidth [TR/TE/BW] = 5000 ms/2.2 ms/490 Hz/pixel, TA = 0:35, field of view [FOV] = 350 mm $\times$ 350 mm) (7,9). After careful calibration of the flip angle in the prostate, SNR maps were calculated from gradient-recalled echo measurements obtained both with and without RF excitation (TR/TE/BW = 200 ms/4.1 ms/300.0 Hz/pixel, TA = 0:53, FOV = 220 mm $\times$ 220 mm, 256 matrix). Anatomic TSE T2WI of the prostate was performed using the above sequence modifications and a variety of spatial resolutions. Finally, for assessment of the potential SNR gain at 7T, SNR was also measured in this volunteer at 3T using a 16-element pelvic-phased array receive coil (Siemens Healthcare, Erlangen, Germany) that is used for standard clinical imaging.

### Patient Evaluation

Two patients with biopsy-proven prostate cancer who were scheduled to undergo radical prostatectomy volunteered to undergo 7T MRI as part of a prospective IRB-approved HIPAA-compliant study and provided written informed consent. Both patients had previously undergone a clinically standard multiparametric prostate MRI study at 3T. The 7T MRI comprised use of the previously described coil arrangement and TSE T2WI sequence, using the above noted sequence modifications. Parameters for axial TSE T2WI at 3T and 7T are provided in Table 1.

Following the 7T MRI, the patients underwent radical prostatectomy using standard surgical technique. The prostate specimen was fixed in formalin for 48 hours, sectioned, and processed using standard hemtoxylin and eosin (H&E) stain. Slides were evaluated by an experienced uropathologist, and tumors outlined in ink. Intact slices were digitally photographed before sectioning, and the sections were digitally scanned (LEICA scanner).

A fellowship-trained abdominal radiologist (A.R., with 5 years of experience in prostate MRI) correlated pathologic findings with the preoperative MRI findings obtained both at 3T and at 7T in both patients. For each patient, a region-of-interest (ROI) was placed within the tumor, ipsilateral and contralateral peripheral zone (PZ), and periprostatic fat, and the mean and standard deviation (SD) recorded. Estimated signal-to-noise ratio (eSNR) was computed for tumor, benign PZ, and periprostatic fat as the ratio between the mean and SD of each of these ROIs, consistent with the method of Heverhagen (10). The SD of air was not used as a marker of image noise given both the lack of air within the included FOV as well as geometric variation in noise across the FOV in the 3T images attributed to use of parallel imaging at this field strength. Tumor-to-PZ contrast was computed as $(SI_{PZ} - SI_{tumor})/(SI_{PZ} + SI_{tumor})$, which provides a value between 0 and 1, with a larger value indicating greater relative contrast. Finally, the homogeneity of benign PZ was calculated as the coefficient of variation in signal intensity between the two lobes (ratio between SD and mean of the signal intensity within the two lobes).

## RESULTS
### Simulations and Phantom Studies

Simulations of the coil system showed that with proper offsetting of the loop transmit elements and application of a $180^{\circ}$ RF phase offset between the two transmit elements, the $B_1^+$ field could be maximized and sufficient uniformity could be achieved in the target ROI (Fig. 2). Mean $B_1^+$ in the prostate was 0.245 A/m/w$^{1/2}$, and $B_1^+$ nonuniformity, measured as standard deviation/mean over the prostate, was 10.4%. Close examination of the $B_1$ vectors through the RF cycle showed that the two loops create a large region of circular polarization in the prostate, enhancing the $B_1^+$ efficiency. Evaluation of the two-loop transmit structure using a body-sized phantom demonstrated that highest transmit efficiency was achieved with the coils offset 4.25 cm from the center, less than had been observed in simulation, and with smaller 12-cm loops. The unloaded-to-loaded Q ratios were 10.3 or better for all coils. Temperature tests conducted using meat allowed establishment of safe SAR limits.

### Volunteer Evaluation

The volunteer was successfully imaged using the described two-loop transmit structure. A $90^{\circ}$ flip angle

could be achieved in the prostate with a 225 v 1 ms hard pulse, 40% above the scanner's usual reference calibration range. Flip angle maps (Fig. 3a) showed good correspondence to the simulated $B_1^+$ fields, with constructive interference creating a reasonably uniform excitation across the ROI, with nonuniformity of 14.1%. SNR maps obtained in the volunteer at 3T and at 7T showed an SNR gain of 2.1 (Fig. 3b). Finally, the TSE T2WI confirmed good depiction of prostate anatomy and clinically relevant details, before planned patient imaging.

### Patient Evaluation

Patient 1 was a 56-year-old male with PSA of 8.1 who, on biopsy, had Gleason 4+3 tumor with maximal tumor involvement of 70% of the core; patient 2 was a 53-year-old male with PSA of 17.7 who, on biopsy, had Gleason 4+3 tumor with maximal tumor involvement of 20% of the core. Both patients successfully underwent 7T MRI using the described coil structure and high-resolution TSE T2WI sequence. This examination demonstrated a focal region of decreased T2 signal in the peripheral zone suspicious

for tumor in both patients. In patient 1, the suspicious area was located in the right posterolateral peripheral zone (Fig. 4a); in patient 2, the suspicious area was located in the left posterolateral peripheral zone (Fig. 5a). In each case, the suspicious area abutted the overlying prostate capsule, which appeared intact without evidence of extraprostatic extension.

Following prostatectomy, pathologic analysis of the specimen demonstrated a dominant Gleason 3+4 tumor in the posterior right apical peripheral zone without extraprostatic extension in patient 1 (Fig. 4b), and a dominant Gleason 3+4 tumor in the posterior left midgland peripheral zone without extraprostatic extension in patient 2 (Fig. 5b). Thus, in both cases, there was good correspondence between findings on 7T T2WI and histopathologic assessment in terms of these aspects of the dominant peripheral zone tumor.

Table 2 provides a comparison of parameters reflecting image quality between 3T an 7T. On average in these two patients, the 7T images demonstrated higher eSNR in both the tumor and the benign PZ, yet lower eSNR in the periprostatic fat. In addition, the 7T images demonstrated slightly decreased tumor-to-PZ
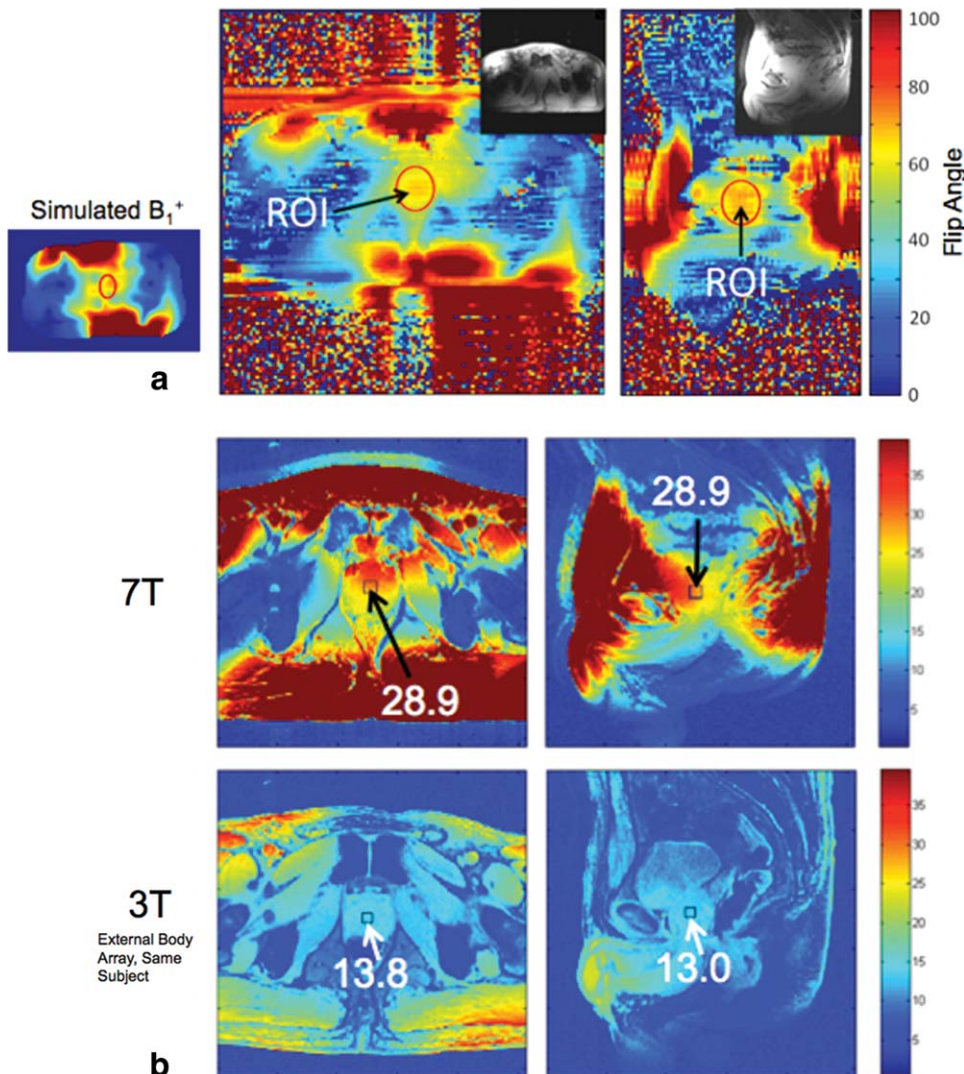


**Figure 3.** Evaluation of two-loop system in healthy volunteer. **a:** Flip angle map (axial slice on left; sagittal slice on right) shows good correspondence to simulated $B_1^+$ field with constructive interference creating reasonable uniform excitation across the area of interest. **b:** Maps of root sum-of-squares signal-to-noise ratio at 7T and 3T demonstrate SNR gain of 3.3 at 7T.
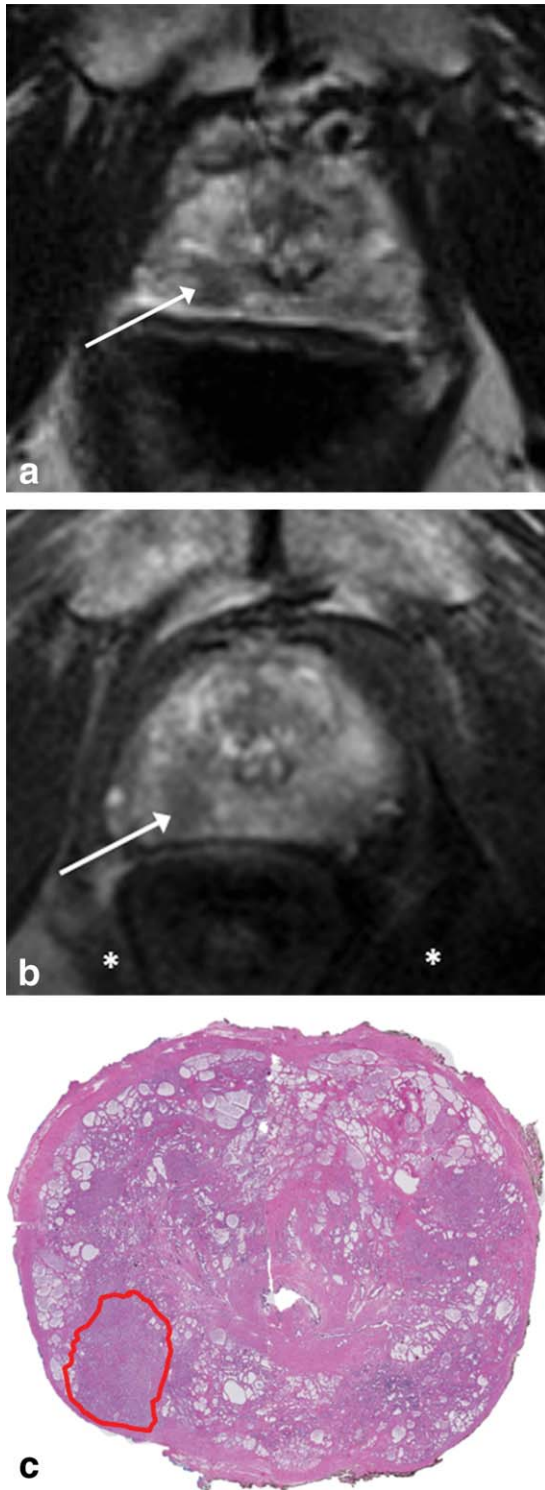
**Figure 4.** Comparison of T2-weighted images of prostate tumors at different field strengths in same subject. **a:** Axial T2-weighted MR image obtained at 3T shows focal area of decreased T2 signal within the right posterior apical peripheral zone (arrow). **b:** Axial T2-weighted MR image obtained at 7T using simplified coil and sequence scheme shows decreased T2 signal in same region, abutting an intact overlying prostate capsule (arrow). Periprostatic fat shows predominantly reduced T2 signal (asterisk). **c:** Reconstructed whole-mount photomicrograph (H&E stain) shows dominant tumor in right posterior peripheral zone outlined in red, corresponding with focal lesion on MRI. No extraprostatic extension was identified on histopathologic assessment. [Color figure can be viewed in the online issue, which is available at wileyonlinelibrary.com.]
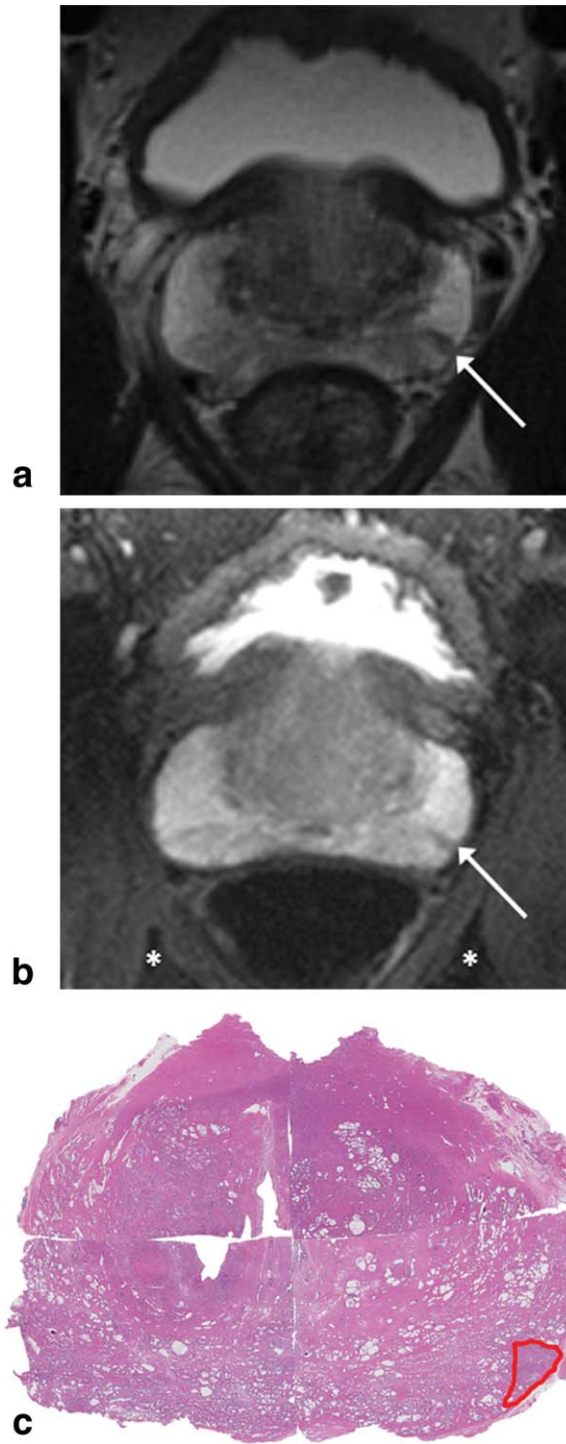
**Figure 5.** Comparison of T2-weighted images of prostate tumors at different field strengths in same subject. **a:** Axial T2-weighted MR image obtained at 3T shows focal area of decreased T2 signal within the left posterior midgland peripheral zone (arrow). **b:** Axial T2-weighted MR image obtained at 7T using simplified coil and sequence scheme shows decreased T2 signal in same region, abutting an intact overlying prostate capsule (arrow). Periprostatic fat shows predominantly reduced T2 signal (asterisk). **c:** Reconstructed whole-mount photomicrograph (H&E stain) shows dominant tumor in left posterior peripheral zone outlined in red, corresponding with focal lesion on MRI. No extraprostatic extension was identified on histopathologic assessment. [Color figure can be viewed in the online issue, which is available at wileyonlinelibrary.com.]

Table 2
Comparison of Axial T2WI of the Prostate at 3T and 7T*

| Field strength | Voxel size | Imaging time | Tumor eSNR | PZ eSNR | Fat eSNR | Tumor-to-PZ contrast | PZ homogeneity (%) |
|---|---|---|---|---|---|---|---|
| 3T | $0.70 \times 0.70 \times 3.0$ | 5min 8s | 7.5 | 16.2 | 11.3 | 0.42 | 11.5 |
| 7T | $0.75 \times 0.75 \times 3.0$ | 3min 19s | 12.8 | 23.3 | 7.9 | 0.34 | 14.0 |

*Tumor and PZ estimated SNR (eSNR), as well as tumor-to-PZ contrast and PZ heterogeneity, represent average value of two patients.

contrast and slightly lower homogeneity of benign PZ compared with 3T images.

## DISCUSSION

The higher SNR of 7T MRI offers the possibility of pursuing intriguing new contrast mechanisms for prostate cancer evaluation. However, performance of novel techniques as a component of a full prostate MRI examination at 7T requires development of the ability to implement standard clinical sequences as well. Greater RF transmitter inhomogeneity and power deposition at 7T preclude use of a whole-body transmit coil, as is the norm at lower field strengths. The alternative approach of using small local transmit coil elements also remains a challenge, still requiring at this point extensive hardware and software development and optimization.

In this development and feasibility study, we presented our approach in the optimization of an external coil array structure for in vivo prostate MRI at 7T. Our solution uses a simple coil structure that avoids the relatively extensive hardware requirements and complicated data acquisition strategies of a coil arrangement that has been previously described for prostate MRI in volunteers at 7T (5,6). The lack of parallel transmission and RF shimming considerably simplifies equipment requirements and makes 7T prostate imaging possible on standard single transmitter 7T systems.

Following further sequence optimization, TSE T2WI was performed in two prostate cancer patients using the simple coil arrangement. In these cases, the tumors were readily visible as a hypointense lesion on T2WI at 7T in both patients. In addition, while both lesions abutted the capsule, the 7T T2WI correctly indicated the absence of extraprostatic extension in both patients, as borne out by histopathologic assessment of the radical prostatectomy specimen. While these two cases demonstrate the feasibility of our hardware and software design for performing high spatial-resolution nonendorectal coil T2WI at 7T for tumor evaluation, differences were noted in comparison with preoperative 3T images in these two patients. As expected, eSNR in the PZ and the tumors was higher at 7T. However, the reduction in eSNR in periprostatic fat was not anticipated and may have implications if using 7T MRI for local staging of prostate cancer, for instance if attempting to determine the presence of extraprostatic extension or neurovascular bundle invasion by tumor. In addition, despite the increased eSNR, tumor-to-PZ contrast and PZ hetero-

geneity were slightly decreased at 7T, indicating the need for continued sequence optimization in a clinical setting.

As we have evaluated our developed coil structure in two patients, further testing and development in additional prostate cancer patients is clearly required. As noted above, the T2WI will warrant continued optimization to maximize diagnostic performance. In addition, the potential impact of 7T imaging on evaluation for tumors of varying size, grade, and location within the prostate must be systematically explored, as it is possible that identification of different subsets of tumors may be influenced by alterations in T2 contrast at the higher field strength. Also for the 7T examination to replace clinical prostate studies at 1.5T or 3T, functional sequences will need to be developed for 7T prostate MRI to complement the T2WI performed in this report. The higher field strength has potential to improve the performance of currently used functional sequences such as MR spectroscopy by means of greater spectral separation of different metabolites, as well as of dynamic contrast-enhanced MRI by means of higher temporal resolution.

In conclusion, work was performed toward optimization of a 7T coil arrangement for prostate MRI at 7T. Our system uses two transmit-receive elements and six receive-only elements, avoiding parallel transmission and RF shimming, thereby achieving a much simpler design than has been previously explored for 7T prostate MRI. This coil design was supplemented by investigation of sequence modifications to overcome challenges related to RF power availability at 7T. In combination, these hardware and software changes led to substantial improvements in SNR compared with 3T MRI. However, continued sequence optimization and testing in larger patient populations remain required.

## REFERENCES

1. Hoeks CM, Barentsz JO, Hambrock T, et al. Prostate cancer: multiparametric MR imaging for detection, localization, and staging. Radiology 2011;261:46–66.
2. Bonekamp D, Jacobs MA, El-Khouli R, Stoianovici D, Macura KJ. Advancements in MR imaging of the prostate: from diagnosis to interventions. Radiographics 2011;31:677–703.
3. Li X, de Moortele V, Ugurbil U, Metzger G. Dynamically applied multiple $B_1^+$ shimming scheme for arterial spin labelling of the prostate at 7T. In: Proceedings of the 19th Annual Meeting of ISMRM, Montreal, Canada, 2011. (abstract 593).
4. van Uden MJ, Veltien A, Scheenen TW, Heerschap A. Design of a double tuned TxRx 1H/31P endorecdtal prostate coil for 7T. In: Proceedings of the 18th Annual Meeting of ISMRM, Stockholm, Sweden, 2010. (abstract 3904).
5. Metzger GJ, Snyder C, Akgun C, Vaughan T, Ugurbil K, Van de Moortele PF. Local $B_1^+$ shimming for prostate imaging with

transceiver arrays at 7T based on subject-dependent transmit phase measurements. Magn Reson Med 2008;59:396–409.

6. Metzger GJ, van de Moortele PF, Akgun C, et al. Performance of external and internal coil configurations for prostate investigations at 7 T. Magn Reson Med 2010;64:1625–1639.

7. Wiggins G, Zhang B, Duan Q, et al. 7 Tesla transmit-receive array for carotid imaging: simulation and experiment. In: Proceedings of the 17th Annual Meeting of ISMRM, Honolulu, Hawaii, 2009. (abstract 394).

8. Duan Q, Sodickson DK, Lattanzi R, Bei Z, Wiggins G. Optimizing 7T spine array design through offsetting of transmit and receive elements and quadrature excitation. In: Proceedings of the 18th Annual Meeting of the ISMRM, Stockholm, Sweden, 2010. (abstract 50).

9. Klose U. Mapping of the radio frequency magnetic field with a MR snapshot FLASH technique. Med Phys 1992;19:1099–1104.

10. Heverhagen JT. Noise measurement and estimation in MR imaging experiments. Radiology 2007;245:638–639.